

# A real space auxiliary field approach to the BCS-BEC crossover

Sabyasachi Tarat and Pinaki Majumdar

Harish-Chandra Research Institute, Chhatnag Road, Jhusi, Allahabad 211019, India

(Dated: 2 Feb 2014)

The BCS to BEC crossover in attractive Fermi systems is a prototype of weak to strong coupling evolution in many body physics. While extensive numerical results are available, and several approximate methods have been developed, most of these schemes are unsuccessful in the presence of spatial inhomogeneity. Such situations call for a real space approach that can handle large spatial scales and retain the crucial thermal fluctuations. With this in mind, we present comprehensive results of a real space auxiliary field approach to the BCS to BEC crossover in the attractive Hubbard model in two dimensions. The scheme reproduces the Hartree-Fock-Bogoliubov ground state, and leads to a  $T_c$  scale that agrees with quantum Monte Carlo estimates to within a few percent. We provide results on the  $T_c$ , amplitude and phase fluctuations, density of states, and the momentum resolved spectral function over the entire interaction and temperature window. We suggest how the method generalises successfully to the presence of disorder, trapping, and population imbalance.

## I. INTRODUCTION

The BCS to BEC crossover in attractive fermion systems is a topic of enduring interest<sup>1</sup>. With increasing interaction, the ground state of a weak coupling ‘BCS superconductor’<sup>2</sup>, with pair size  $\xi$  much larger than the interparticle separation  $k_F^{-1}$ , evolves smoothly<sup>3-5,7,8</sup> into a ‘Bose-Einstein condensate’ (BEC) of preformed fermion pairs with  $\xi \lesssim k_F^{-1}$ .  $k_F$ , above, is the Fermi wavevector. The ‘high temperature’ normal state changes from a conventional Fermi liquid at weak coupling to a gapped phase at strong coupling. While the zero temperature pairing gap increases with coupling strength, the superconducting  $T_c$  in lattice systems reaches a maximum at intermediate coupling and falls thereafter. A striking consequence of the separation of pairing and superconducting scales is the emergence of a (pseudo)gapped normal phase, with preformed fermion pairs but no superconductivity due to strong phase fluctuations.

The early work of Leggett<sup>4</sup> and Nozieres and Schmitt-Rink<sup>5</sup> provided the intuitive basis for understanding this problem. It has since been followed up by powerful semi-analytic schemes<sup>9-13</sup>, extensive quantum Monte Carlo (QMC) work<sup>14-23</sup>, and most recently dynamical mean field theory (DMFT)<sup>25-30</sup>. The efforts have established the non-monotonic  $T_c$ , and the presence of a pseudogap in the single particle spectrum beyond moderate coupling and temperature  $T > T_c$ .

While the success of multiple methods in capturing the crossover is remarkable, most of them depend on translation invariance in the underlying problem. They do not naturally generalise to problems that involve the presence of disorder, or a confining potential, or the emergence of spontaneous modulation. These situations, for example, occur in the context of the disorder driven superconductor-insulator transition<sup>31</sup>, trapped fermions in an optical lattice<sup>32</sup>, and Fulde-Ferrell-Larkin-Ovchinnikov (FFLO) states<sup>33</sup> in population imbalanced systems. Such problems, in general, require a real space approach. This paper presents such a real space implementation based on a static auxiliary field (SAF) scheme.

Our main results are the following: (i) We demonstrate the ability of our approach to quantitatively capture the  $T_c$  scale across the BCS-BEC crossover, confirming its usefulness at all interaction strengths. (ii) We quantify the crossover from an amplitude fluctuation dominated regime to a phase fluctuation dominated regime, through the ‘high  $T_c$ ’ intermediate coupling window where both are important. (iii) We present the thermal evolution of the single particle density of states with interaction and temperature, and, more importantly, the momentum resolved spectral function  $A(\mathbf{k}, \omega)$ . We compare our results to QMC data wherever available.

The paper is organised as follows. In Sec.II we quickly compare the existing analytic and numerical methods used to study the BCS-BEC crossover in lattice models. Sec.III presents our model and describes the method used in detail. Sec.IV shows our results on thermodynamic indicators, the nature of fluctuations, density of states, and  $A(\mathbf{k}, \omega)$ . Sec.V discusses the limitations of our method and the scope for further work.

## II. EARLIER WORK

Since the BCS-BEC crossover is a prototype of weak to strong coupling evolution, several methods, of increasing sophistication, have been brought to bear on it. These include mean field theory (MFT)<sup>4</sup>, MFT corrected by gaussian fluctuations<sup>5</sup>, the self consistent T-matrix approach (SC-TMA)<sup>9,10</sup>, a two particle self consistent (2PSC) scheme<sup>11</sup>, the mapping to XY models<sup>12,13</sup>, quantum Monte Carlo (QMC)<sup>14-23</sup>, and recently dynamical mean field theory (DMFT)<sup>25-30</sup>.

There are detailed descriptions of these methods available in the original literature so we just provide a table that compares the strengths and limitations of these methods in the light of a few crucial indicators. These in our opinion include (i) thermodynamics:  $T_c(U)$ , (ii) single particle spectra, (iii) two particle properties, *e.g.* conductivity, and (iv) handling inhomogeneity, *e.g.* disorder or trapping.

Method	$T_c(U)$	Spectra at large $U/t$	Transport at large $U/t$	Handling inhomogeneity
MFT	Correct only when $U/t \lesssim 1$ .	No gap/pseudogap in the normal state.	No access to transport.	Real space MFT is reasonable at $T = 0$ , can access size $\sim 40 \times 40$ .
MFT+fluctuations	No results on the full $T_c(U)$ in the lattice model.	PG above mean field $T_c$ , incapable of capturing BKT physics <sup>6</sup>	No results	Not systematically explored.
SC-TMA	Accurate upto intermediate coupling; captures non monotonic behaviour correctly to $U \sim 8$ . <sup>9</sup>	Shows a PG, but quantitatively inaccurate due to neglect of vertex corrections <sup>6</sup> .	No results	Not generalised.
2PSC	Fluctuations drive $T_c$ to zero <sup>6</sup> .	Accurate upto intermediate coupling <sup>11</sup> .	No results	Not generalised.
XY models	Captures non monotonic $T_c(U)$ but not quantitatively accurate <sup>12,13</sup> .	PG inferred from different pairing and $T_c$ scales.	Not explored.	Disordered XY model needs to be derived from the Hubbard model.
QMC	Accurate, sets the benchmark <sup>15,23</sup> .	Accurate in principle but involves uncertainties due to analytic continuation from imaginary frequencies <sup>16,20</sup> .	Contains the relevant physics but dynamical properties are difficult to extract due to analytic continuation.	Handles inhomogeneity <sup>24</sup> but sizes limited to $\sim 12 \times 12$ . Limited to $U \gtrsim 4t$ .
DMFT	Captures non monotonic $T_c(U)$ but quantitatively inaccurate when used in the 2D context <sup>25</sup> .	Accurate <sup>29</sup> .	Transport misses bosonic contribution.	Requires <i>ad hoc</i> real space generalisation.
SAF	Accurate, matches quantitatively with QMC.	Accurate, compares reasonably with QMC.	Transport misses bosonic contribution.	Handles inhomogeneity, $\mathcal{O}(N)$ method, readily accesses size $\sim 30 \times 30$ <sup>41</sup> .

TABLE I. Comparison of earlier work with our method

### III. MODEL AND METHOD

We study the attractive two dimensional Hubbard model (A2DHM),

$$H = \sum_{ij,\sigma} (t_{ij} - \mu \delta_{ij}) c_{i\sigma}^\dagger c_{j\sigma} - |U| \sum_i n_{i\uparrow} n_{i\downarrow}$$

For us  $t_{ij}$  denotes nearest neighbour tunneling amplitude  $t$  on a square lattice.  $\mu$  is the chemical potential. We set  $t = 1$  and measure all other energies in terms of it.  $U > 0$  is the strength of onsite Hubbard attraction. We will focus on the density  $n \sim 0.9$  which is close to half-filling but avoids the density wave features of  $n = 1$ .

The model is known to have a superconducting ground state for all  $n \neq 1$ , while at  $n = 1$  there is the coexistence of superconducting and density wave (DW) correlations in the ground state. For  $n \neq 1$  the ground state evolves from a BCS state at  $U/t \ll 1$  to a BEC of ‘molecular pairs’ at  $U/t \gg 1$ . The pairing amplitude and gap at  $T = 0$  can be reasonably accessed within mean field theory or a simple variational wavefunction.

Mean field theory, however, assumes that the electrons are subject to a *spatially uniform* self-consistent pairing amplitude  $\langle\langle c_{i\uparrow}^\dagger c_{i\downarrow}^\dagger \rangle\rangle$ . At small  $U/t$  this vanishes

when  $k_B T \sim t e^{-t/U}$ , but at large  $U/t$  it vanishes only when  $k_B T \sim U$ . The actual  $T_c$  at large  $U$  is controlled by phase correlation of the local order parameter, rather than finite pairing amplitude, and occurs at  $k_B T_c \sim f(n)t^2/U$ , where  $f(n)$  is a function of the density. The wide temperature window, between the ‘pair formation’ scale  $k_B T_f \sim U$  and  $k_B T_c$  corresponds to equilibrium between unpaired fermions and hardcore bosons (paired fermions).

We use an auxiliary field scheme, based on the Hubbard-Stratonovich (HS) transformation, to retain the thermal amplitude and phase fluctuations explicitly. Formally, the HS transformation (below) allows us to recast the original interacting problem into that of electrons coupled to space-time fluctuating auxiliary fields. Usually the auxiliary fields are *either* the ‘pairing fields’  $\{\Delta_i(\tau), \Delta_i^*(\tau)\}$  *or* a ‘density’ field  $\phi_i(\tau)$ . The pairing field based decomposition is employed in the Bogoliubov-de Gennes (BdG) approach, while QMC uses the density based decomposition.

While these two representations lead to the same answer when the resulting problem is treated exactly, any approximation leads to answers that are decomposition dependent. ‘Single channel’ decompositions<sup>34,37</sup>, above, have the shortcoming that they *do not* reproduce the

conserving Hartree-Fock-BdG (HFBdG) theory in their static limit, crucial when density inhomogeneities are present.

Following recent suggestions<sup>36</sup> we rewrite the A2DHM in terms of *classical* auxiliary fields in *both* pairing and density channels, see below, so that the saddle point reproduces HFBdG theory.

$$H_{eff} = H_{kin} + \sum_i (\Delta_i c_{i\uparrow}^\dagger c_{i\downarrow}^\dagger + h.c.) - \sum_i \phi_i n_i + \sum_i \frac{|\Delta_i|^2}{U} + \sum_i \frac{\phi_i^2}{U} \quad (1)$$

We treat the  $\{\Delta_i, \Delta_i^*, \phi_i\}$  as time independent, *i.e.* classical fields. The partition function is:

$$Z = \int \mathcal{D}\Delta\Delta^*\mathcal{D}\phi Tr_{c,c^\dagger} e^{-\beta H_{eff}}$$

As  $T \rightarrow 0$ , it is obvious that  $Z$  will be dominated by the saddle point configuration, *i.e.*  $\Delta_i, \phi_i$ , that minimise  $H_{eff}$ . Thus at  $T = 0$ :  $\Delta_i = U \langle c_{i\uparrow} c_{i\downarrow} \rangle$ ,  $\phi_i = \frac{U}{2} \langle n_i \rangle$ . These minimum conditions are easily recognised as the self-consistency requirements of HFBdG theory. Minimising  $H_{eff}$  is thus the same as solving the Bogoliubov-de Gennes (BdG) equations. While this is good, we want to capture the thermal physics as well.

At finite  $T$  the BdG approach would promote the consistency condition above to thermal averages, and the electrons would see only the *average* background at any temperature. It is easy to see the limitation of this approach when we consider the clean problem at large  $U$ . Since the system is translation invariant, averages like  $\langle c_{i\uparrow}^\dagger c_{i\downarrow}^\dagger \rangle$  are site independent. Their self-consistent value, and hence superconductivity, vanishes when  $T \sim U$ , way above the correct  $T_c \sim t^2/U$ . To remedy this we need to *average the electron motion over disordered thermal configurations* rather than solve for electron motion in the disorder averaged configuration.

The Boltzmann weight for the occurrence of a particular  $\{\Delta_i, \phi_i\}$  configuration is

$$P\{\Delta_i, \phi_i\} \propto Tr_{c,c^\dagger} e^{-\beta H_{eff}} \quad (2)$$

This is related to the electron free energy in a particular  $\{\Delta_i, \phi_i\}$  background. If the fields are large and random the trace cannot be analytically computed. We generate the equilibrium  $\{\Delta_i, \phi_i\}$  configurations by a Monte Carlo technique<sup>37,38</sup>. This involves diagonalisation of the electron Hamiltonian  $H_{eff}$  for every attempted update of the auxiliary fields and the Metropolis condition for acceptance of this move. We use a cluster based implementation of the Monte Carlo<sup>40</sup> and can access sizes upto  $32 \times 32$ .

The expectation value of any observable  $f(c_i, c_i^\dagger)$  can then be computed as follows. For each configuration  $\{\Delta_i, \phi_i\}$ , the first step is to express the fermionic operators in terms of the quasiparticle operators  $(\gamma_i, \gamma_i^\dagger)$ , with the HFBdG eigenvectors  $(u_n^i, v_n^i)$  as coefficients. The

electronic trace over the resultant expressions in terms of the quasiparticle operators can be easily evaluated. This final expression is then averaged over all thermal configurations  $\{\Delta_i, \phi_i\}$ . We will describe the indicators separately in detail in their respective sections.

## IV. RESULTS

### A. Thermodynamic indicators

Fig.1.(a) shows our result for the structure factor corresponding to the growth of superconducting order. We compute the thermally averaged pairing field correlation  $S(\mathbf{q}) = \frac{1}{N^2} \sum_{ij} \langle \Delta_i \Delta_j^* \rangle e^{i\mathbf{q} \cdot (\mathbf{r}_i - \mathbf{r}_j)}$  at  $\mathbf{q} = \{0, 0\}$ . This is like the ‘ferromagnetic’ correlation between the  $\Delta_i$ , treating them as two dimensional moments. If the  $\mathbf{q} = \{0, 0\}$  component,  $S(0)$ , is  $\mathcal{O}(1)$  it implies that the pairing field has a non-zero spatial average and would in turn induce long range order (power law correlation in 2D) in the thermal and quantum averaged correlation  $M_{ij} = \langle \langle c_{i\uparrow}^\dagger c_{i\downarrow}^\dagger c_{j\downarrow} c_{j\uparrow} \rangle \rangle$ . We locate the superconducting transition from the rise in  $S(0, T)$  as the system is cooled. The results are not reliable below  $U/t \lesssim 1$ , since the correlation length  $\xi$  becomes comparable to our system size, but compare very well with available QMC data for

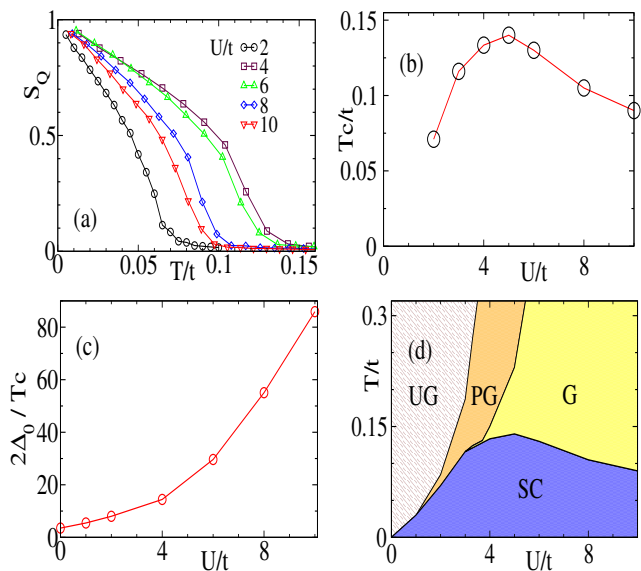


FIG. 1. Colour online: (a). Temperature dependence of the  $\mathbf{q} = \{0, 0\}$  component of the pairing field correlation for different  $U/t$ . The onset locates the superconducting  $T_c$ . (b). The  $T_c$  inferred from the structure factor result. This is compared to QMC results at the end of the paper. (c). Ratio of  $T = 0$  gap  $2\Delta_0$  to  $T_c$ . In the BCS limit the ratio would be  $\sim 3.5$ . (d). The ‘phase diagram’ in terms of the low frequency behaviour of the density of states. The high temperature normal state has three regimes, unpaired (UG), pseudogapped (PG) and gapped (G), while for  $T < T_c$  the system is a gapped superconductor (SC).

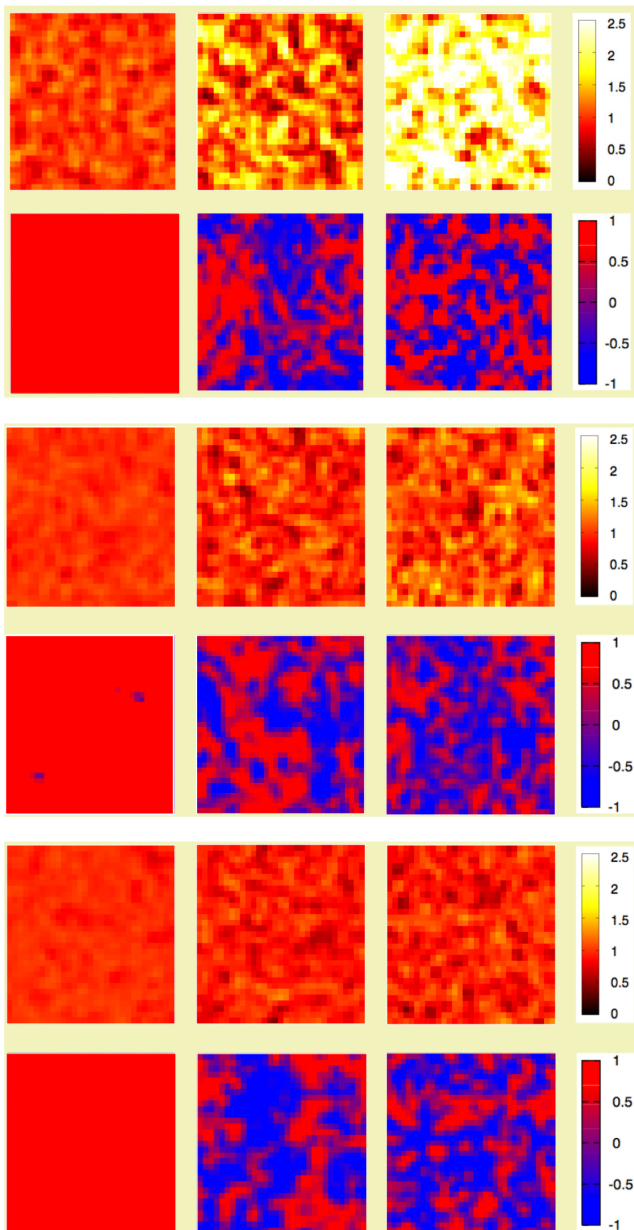


FIG. 2. Colour online: Maps of amplitude fluctuation and phase correlation for single configurations at  $U/t = 2$  (top),  $U/t = 6$  (middle) and  $U/t = 10$  (bottom) at three temperatures:  $T = 0.1T_c$ ,  $T = T_c$  and  $T = 2T_c$  (left to right). For each set, the upper row shows the amplitude  $|\Delta_i|$  (normalised by the  $T = 0$  mean field value  $\Delta_0$ ) for a MC configuration, while the lower row shows the phase correlation:  $\Phi_i = \cos(\theta_i - \theta_0)$ , where  $\theta_0$  is the phase at a site  $\mathbf{R}_0$  near the center.

$U/t \gtrsim 2$ . We will discuss the interpretation of the  $S(0, T)$  results in detail at the end of the paper.

Panel 1.(b) shows the result for  $T_c(U)$  showing the clear peak around  $U/t \sim 5$ . We will compare this to the result from QMC, and also discuss the system size dependence, at the end of the paper.

Panel 1.(c) highlights the rapid rise in the ‘gap’ to  $T_c$  ratio with increasing interaction. In the weak coupling

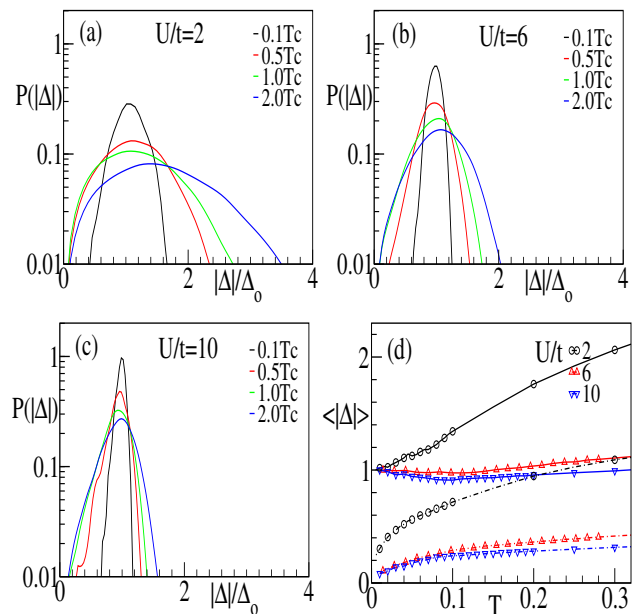


FIG. 3. Colour online: (a)-(c). The distribution  $P(|\Delta|)$  of the magnitude,  $|\Delta|$ , of the pairing field. The x-axis is normalised by the mean field value  $\Delta_0$  at  $T = 0$ . The results are for  $T = 0.1T_c$ ,  $0.5T_c$ ,  $1.0T_c$ ,  $2.0T_c$ . (a).  $U/t = 2$ , (b).  $U/t = 6$ , (c).  $U/t = 10$ . At  $U/t = 2$  there is a prominent increase in the mean and width of  $P(|\Delta|)$  with  $T$ . This  $T$  dependence weakens with growing  $U/t$ . (d). The growth of the mean value and width with  $T$ . The mean is normalised by the  $T = 0$  value. The firm lines denote the mean  $|\Delta|$ , while the dot-dashed lines show the corresponding width.

limit this value is 3.5, at  $U = 2t$  it is already  $\sim 7$ , quite beyond BCS, and grows roughly as  $(U/t)^2$  at large  $U$ . Needless to say, the  $T = 0$  gap is not an indicator of the robustness of the superconducting state once we go beyond weak coupling.

The large gap but low  $T_c$  leaves its imprint on several physical properties. The phase diagram, Fig.1.(d), highlights this. At weak coupling the vanishing of SC order also means the vanishing of the gap in the density of states. The high  $T$  regime at small  $U/t$  is ungapped (UG). The regime  $U/t \lesssim 2$  is a ‘renormalised BCS’ window, although the gap to  $T_c$  ratio is large. For  $2 \lesssim U/t \lesssim 4$  the  $T > T_c$  phase has a pseudogap (PG), which we show in Fig.2, while for  $U/t \gtrsim 4$  the  $T > T_c$  regime is gapped. Notice that the normal state gap appears before the peak  $T_c$  is reached, *i.e.*, on the ‘BCS’ side of the crossover.

## B. Background fields

To understand the spatial behaviour of the system and its evolution with  $U$  and  $T$  we examine the variation of the background fields  $\Delta_i$  and  $\theta_i$ . Fig.2 shows single snapshots of  $|\Delta_i|$  (upper row in each set), normalised by the  $T = 0$  mean field value, and the phase correlation

$\Phi_i = \cos(\theta_i - \theta_0)$  (lower row in each set), where  $\theta_0$  is the angle at fixed site  $R_0$  in the lattice.

Of the three sets in Fig.2, the top set is for  $U/t = 2$ , which we will use as typical of ‘weak’ coupling, the middle set is for  $U/t = 6$ , typical of intermediate coupling, and the top set is for  $U/t = 10$ , strong coupling. The rows are for  $T/T_c(U) = 0.1, 1, 2$ .

At  $T = 0$  all the snapshots show almost uniform  $|\Delta_i|$  and perfect phase locking at all  $U/t$ . This is just the mean field state. As we move to higher  $T$ , however, we see a clear difference in the amplitude fluctuations of the three systems. While the  $U/t = 2$  plots show an increasing inhomogeneity and a steadily rising value of  $\Delta$  throughout the system, the  $U = 10t$  case hardly shows any change. The  $U = 6t$  behaviour is intermediate. This shows that with increasing  $U$ , the system moves smoothly from an amplitude fluctuation dominated regime to one in which amplitudes are effectively constant, the transition being driven by the phase fluctuations.

The phase maps, on the other hand, show how the system breaks up into correlated patches with temperature. The middle column corresponds to  $T_c$ , and show large correlated clusters, as expected for a system close to criticality. As  $T$  is increased, the correlation length decreases, as evident from the right column at  $2T_c$ .

While it is phase fluctuations that ultimately destroy order at all  $U/t$ , the amplitude fluctuations are quantitatively important at weak coupling. To highlight this, we plot the distribution of  $|\Delta|$  for the three  $U$  values at four temperatures  $T = 0.1T_c, 0.5T_c, T_c$  and  $2T_c$  for each  $U$  in Fig.3 (a),(b) and (c). (d) shows the temperature dependence of the mean  $\langle|\Delta|\rangle$  and its variance for  $U = 2t, 6t$  and  $10t$ . We find that the distributions widen for each case with increasing  $T$ , but the increase is much more pronounced at weak coupling, and decreases systematically with increasing coupling. The distribution is noticeably non gaussian at high temperature in the weak coupling case. The temperature dependence of the mean and width of  $P(|\Delta|)$  is shown in Fig.3.(d). A detailed discussion is postponed to the end of the paper.

### C. Density of states

Fig.4 highlights the behaviour of the single particle density of states (DOS). We show results at the ‘BCS end’ ( $U = 2t$ ), near the peak  $T_c$  ( $U = 6t$ ), and in the BEC regime ( $U = 10t$ ). The  $T = 0$  results in all cases are described by the canonical DOS,  $N(\omega) \sim 1/\sqrt{\omega^2 - |\Delta_0|^2}$ , where  $2\Delta_0$  is the full  $T = 0$  gap in the single particle spectrum. There is a gap in the spectrum at all  $U$ , a ‘coherence peak’ at the gap edges, arising from electron propagation in a perfectly pair correlated background, and a featureless fall at high energies. The oscillatory pattern in the DOS at  $T = 0$  for  $U = 2t$  is a consequence of finite size, showing up even on a  $24 \times 24$  lattice.

While the  $T = 0$  DOS is just a mean field result, and the  $T$  dependence at  $U = 2t$  is expected, the  $T$  depen-

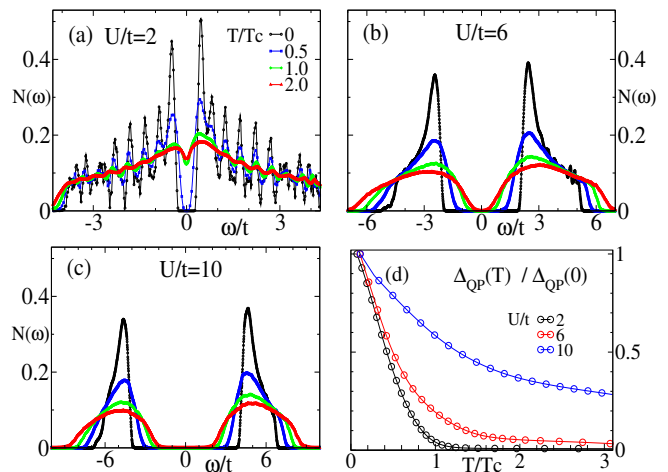


FIG. 4. Colour online: Temperature dependence of the DOS,  $N(\omega)$  at different couplings. Panels (a)-(c) have the same legends. (a).  $U/t = 2$ , (b).  $U/t = 6$ , and (c).  $U/t = 10$ . The oscillations in the DOS in panel (a) are finite size artifacts (even on a  $24 \times 24$  lattice). At  $U/t = 2$  the gap essentially vanishes at  $T \sim T_c$ , while at  $U/t = 6$  a small ‘hard gap’ persists to  $T_c$  and above, although lorentzian broadening gives the impression of a pseudogap at the highest  $T$ . For  $U/t = 10$  a ‘hard gap’ persists to  $T \sim 0.5$  although with a clear reduction with increasing temperature. (d). Variation in the single particle gap, normalised by its  $T = 0$  value.

dence at  $U = 6t$  and  $U = 10t$  is not obvious. At  $U = 6t$ , the system has a ‘hard gap’ persisting to  $T \sim 3T_c \sim 0.5t$ . This is reflected in the phase diagram in Fig.1. At both  $U = 6t$  and  $10t$  the transition to SC occurs from a gapped fermion state rather than a Fermi liquid. The DOS indicates that down to  $U$  values around peak  $T_c$  (and even somewhat below) the qualitative physics remains similar to the BEC end.

Another striking feature is the large transfer of spectral weight that occurs on a modest change of temperature. For the  $U = 10t$  case, for example, at  $T \sim T_c \sim 0.09t$  there is weight transfer over a scale  $\mathcal{O}(U)$ . The reason is fairly simple: the magnitude  $|\Delta_i|$  in this limit are almost  $T$  independent, but the phase correlation between them is destroyed at a temperature  $T \sim t^2/U$ . As a result, over a small  $T$  window the system evolves from a state with perfectly ordered  $\Delta_i$ , to one where these large amplitudes are randomly oriented. The strong ‘disorder’ in the  $\Delta_i$  lead to the broadening of the density of states.

The large size of  $|\Delta_i|$  even in the normal state preserves the gap feature, but the randomness smears the band edges.

### D. Spectral functions

Now we turn to the spectral functions. Fig.5 shows intensity plots of the spectral function  $A(\mathbf{k}, \omega)$  for  $U/t = 2, 6, 10$  (top to bottom) for  $T/T_c = 0.1, 1, 2$  (left to right). Let us start with the low temperature results,

where mean field theory is a good starting point.

Our density  $n \sim 0.9$  involves a non interacting Fermi surface that is almost a square and rotated by  $45^\circ$  with respect to the Brillouin zone. So, the separation between the two branches,  $\pm\sqrt{(\epsilon_{\mathbf{k}} - \mu)^2 + \Delta_0^2}$ , of the mean field dispersion is smallest near  $(0, \pi)$  and  $(\pi/2, \pi/2)$ . Within MFT the spectral function is given by  $A(\mathbf{k}, \omega) = u_{\mathbf{k}}^2 \delta(\omega - E_{\mathbf{k}}) + v_{\mathbf{k}}^2 \delta(\omega + E_{\mathbf{k}})$ . In the BCS limit,  $v_{\mathbf{k}}^2$  is either one or zero for  $k < k_F$  or  $k > k_F$ , with a small region around  $k_F$  where it crosses from one to the other.

At  $U = 2t$ ,  $v_{\mathbf{k}}^2 \sim 1$  for  $\epsilon_{\mathbf{k}} \lesssim \mu$ , and  $u_{\mathbf{k}}^2 \sim 1$  for  $\epsilon_{\mathbf{k}} \gtrsim \mu$ , with significant mixing only near  $\mu$ . As a result  $A(\mathbf{k}, \omega)$  shows either a lower branch or an upper branch, but not both - except for  $\epsilon_{\mathbf{k}} \sim \mu$ .

The growing symmetry in the plots, about the horizontal  $\omega = 0$  line, with increasing  $U/t$  arises from the changing character of  $u_{\mathbf{k}}$  and  $v_{\mathbf{k}}$ . For  $U/t \gg 1$ ,  $u_{\mathbf{k}}^2$  and  $v_{\mathbf{k}}^2$  are both  $\sim 1/2$  all over the Brillouin zone, since ‘pairing’ is no longer limited to the vicinity of the non interacting

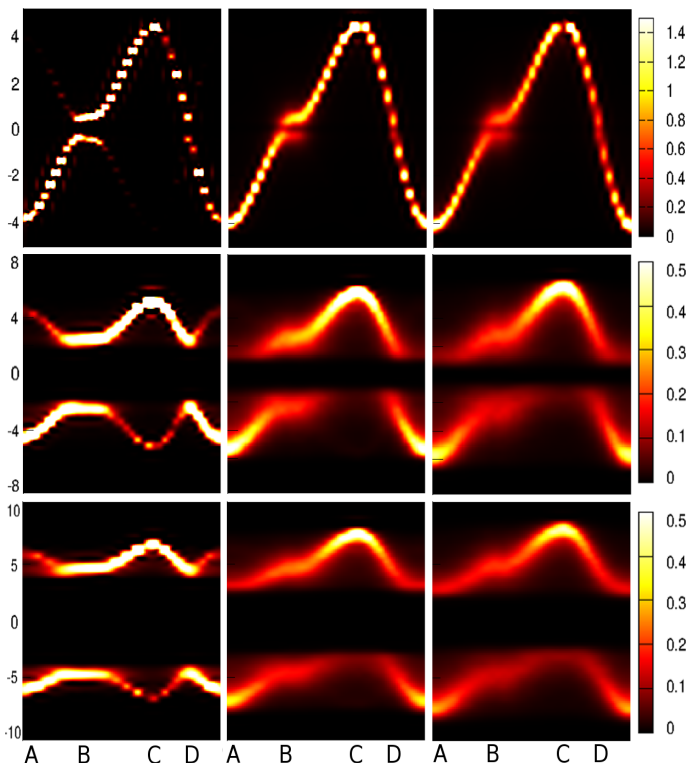


FIG. 5. Colour online: Plot of  $A(\mathbf{k}, \omega)$ . The rows, left to right, are for  $U/t = 2, 6$  and  $10$ . Columns, top to bottom, correspond to  $0.1T_c, T_c$  and  $2T_c$ . The momentum, on the x-axis, is scanned as  $(0,0) \rightarrow (0,\pi) \rightarrow (\pi,\pi)$  and back through  $(\pi/2,\pi/2)$  to  $(0,0)$  along the diagonal. These points are labelled as A, B, C and D respectively. The gaps are lowest around  $(\pi/2, \pi/2)$  and  $(\pi, 0)$ , where the Fermi-surface of the free system intersects our path in  $k$ -space. Increasing temperature causes broadening and a decrease of the gaps, which close in the case of  $U = 2t$ . The increasing symmetry of the low  $T$  graphs with increasing  $U$  signals the participation of states far from the FS in pairing.

Fermi surface (FS). The cases  $U = 6t$  and  $U = 10t$  are already in this regime although some residual asymmetry is visible. The large difference between weak and strong coupling in terms of the  $T = 0$  pairing amplitude decides the finite  $T$  state.

At finite  $T$ , thermal fluctuations broaden the delta functions and the detailed lineshapes for  $\mathbf{k} = \{\pi, \pi\}$  and  $\{\pi/2, \pi/2\}$  are shown in Fig.6. As expected, the gap closes for  $U = 2t$ , while it does not for  $U = 6t$  and  $U = 10t$ , though there is a noticeable decrease in the former.

Quantum Monte Carlo work<sup>20</sup> had suggested the presence of non-trivial structure in the spectral function near the zone boundary  $(\pi, \pi)$ . The top row in Fig.6 shows the spectral function at this  $\mathbf{k}$  point for  $U/t = 2, 6, 10$  at three temperatures,  $T = 0.5T_c, T_c, 2T_c$ . The energy is measured in units of the  $T = 0$  dispersion  $E_{\mathbf{k}}^0$ .

We start with the top row:  $\mathbf{k} = \{\pi, \pi\}$ . At high temperature the  $U = 2t$  case shows only a single broad peak at positive energy, whereas  $U/t = 6, 10$  show a second peak at a smaller negative energy value. This two peak structure with a gap around  $\omega = 0$  is an indicator of pairing without global coherence. The complete absence at  $U = 2t$ , and the increase in peak height from  $U = 6t$  to  $10t$  bolsters this interpretation.

We do not find any peak near  $\omega \sim 0$  for medium to large  $U$ . However from  $T_c$  downwards, another peak becomes visible at negative energies, at  $\omega \sim -E_{\mathbf{k}}^0$ . This peak is indicative of the global coherence setting in below  $T_c$ . As  $T$  is decreased, this peak slowly gains weight while weight in the ‘pairing feature’ becomes smaller, with its maximum shifts to larger negative energies as the gap becomes larger.

Thus, we find some degree of consistency with the QMC work which mainly deals with temperatures larger than  $T_c$ , and also find another peak, indicative of global coherence, that starts to develop below  $T_c$ .

For  $\mathbf{k} = \{\pi/2, \pi/2\}$  and high temperature the spectral functions at  $U = 6t$  and  $U = 10t$  have a gap at  $T > T_c$ , as before, while the  $U = 2t$  result is gapless. In contrast to  $\mathbf{k} = \{\pi, \pi\}$  however we cannot disentangle the lower temperature coherence feature, at  $\omega = \pm E_{\mathbf{k}}^0$  from the overall broad band.

## V. DISCUSSION

Our model has been set up with the explicit constraint that it reproduce the standard mean field (or HFBdG) result at  $T = 0$ . It ignores quantum fluctuations of the pairing field. The impact of these fluctuations have been discussed using DMFT by Garg et. al.<sup>27</sup> and Bauer and Hewson<sup>28</sup>. They find that the *qualitative* results for the order parameter, spectral gap, occupation probability and superfluid stiffness are all given correctly by the mean field method, though it tends to overestimate the spectral gaps and order parameter values at intermediate coupling. For most of the  $U$  window, however, the mean

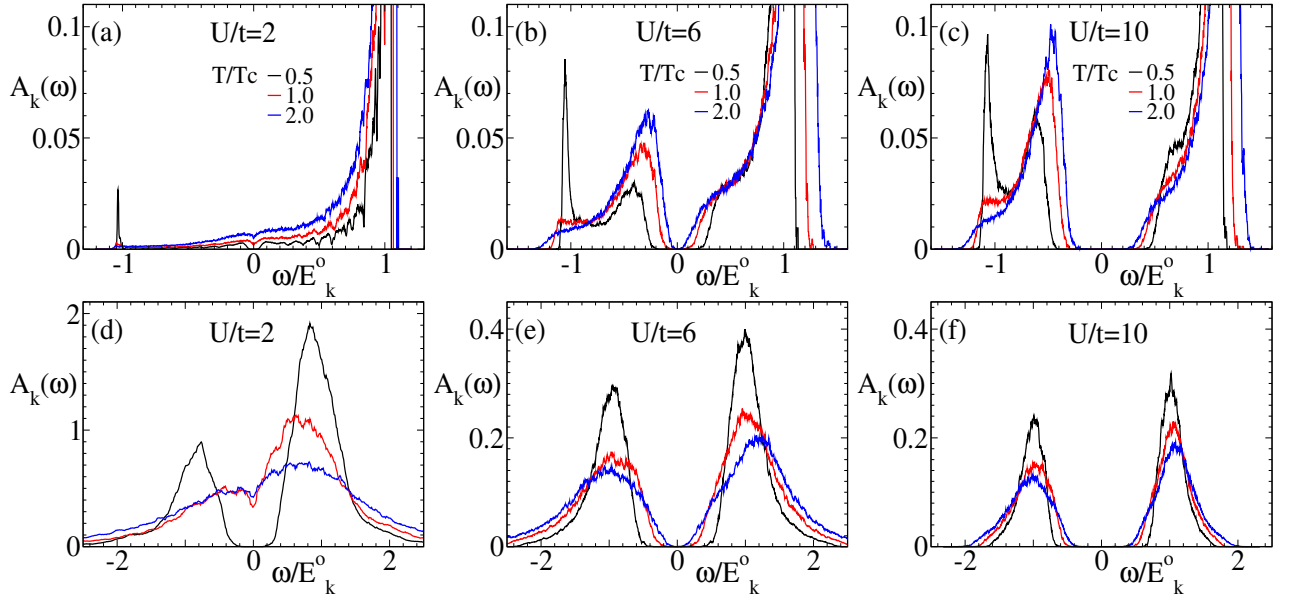


FIG. 6. Colour online: Spectral function  $A(\mathbf{k}, \omega)$ . The panels in the top row are for  $\mathbf{k} = \{\pi, \pi\}$ . (a).  $U/t = 2$ , (b).  $U/t = 6$ , (c).  $U/t = 10$ . Bottom row,  $\mathbf{k} = \{\pi/2, \pi/2\}$ , and interaction strengths: (d).  $U/t = 2$ , (e).  $U/t = 6$  and (f).  $U/t = 10$ . For each  $U$  we show data at  $T = 0.5T_c, T_c$  and  $2T_c$ . The frequency axis is normalised by the  $\mathbf{k}$  dependent mean field energy  $E_{\mathbf{k}}^0$  at  $T = 0$ . For  $\mathbf{k} = \{\pi, \pi\}$ , which is outside the non interacting Fermi surface, the basic structure consists of large peak at positive energies  $\omega \sim E_{\mathbf{k}}^0$ , a broad negative energy feature at  $\omega \gtrsim -E_{\mathbf{k}}^0$ , and for  $T < T_c$  a remnant of the QP peak at  $\omega = -E_{\mathbf{k}}^0$ . Beyond weak coupling the survival of a two peak structure even for  $T > T_c$  indicates ‘incoherent pairs’. For  $\mathbf{k} = \{\pi/2, \pi/2\}$  the features are similar to what we observe at  $\mathbf{k} = \{\pi, \pi\}$ , except the QP peak is no longer separately visible.

field results are reasonable. The results from our method should get better at finite temperature as thermal fluctuations become more important than zero point quantum fluctuations. A comparison of our  $T_c$  with QMC estimate bears this out.

*Accuracy of  $T_c$  estimate:* Fig. 7(a) compares our  $T_c$  with different methods. We find that our results compare well with QMC and sophisticated semi-analytic methods with a slight underestimate at medium to large coupling. Fig.8(b) shows the size dependence of the  $T_c$  estimate with data for  $L = 8, 16, 24$ . We see that while the ‘critical temperature’ decreases noticeably from  $L = 8$  to 16, it does not change significantly beyond  $L = 16$ . Thus, the estimate we obtain at  $L = 24$  should be a fair approximant to the bulk  $T_c$ .

*Effective classical functional:* The BdG framework involves fermions coupled to the fields  $\Delta_i$  and  $\phi_i$ . For simplicity let us focus on the  $\Delta_i$  since the  $\phi_i$  do not play a crucial role in a translation invariant system.

The physics of fermions in an arbitrary  $\Delta_i$  background is not obvious. It is therefore helpful to have an explicit classical functional involving only the  $\Delta_i$  since the minimum and possible fluctuations in  $\Delta_i$  are easier to estimate.

If the  $\Delta_i$  are small compared to the kinetic energy, as would happen when  $U/t \ll 1$ , the functional,  $H_{eff}^0$ , can be obtained via a standard cumulant expansion:

$$H_{eff}^0\{\Delta_i\} = \sum_{ij} a_{ij} \Delta_i \Delta_j^* + \sum_{ijkl} b_{ijkl} \Delta_i \Delta_j^* \Delta_k \Delta_l^* + \mathcal{O}(\Delta^6)$$

The superscript in  $H_{eff}$  is to indicate  $U/t \ll 1$  character.  $a_{ij} = -\chi_{ij}^0/2 + (1/U)\delta_{ij}$ ,  $\chi_{ij}^0$  being the non-local pairing susceptibility of the free Fermi system, and  $b_{ijkl}$  can be computed from a convolution of four free Fermi Greens functions.

If we had  $U/t \gg 1$  then  $H_{eff}$  would have to be expanded to higher order in  $\Delta_i$ . In that situation it actually helps to extract the functional by expanding in powers

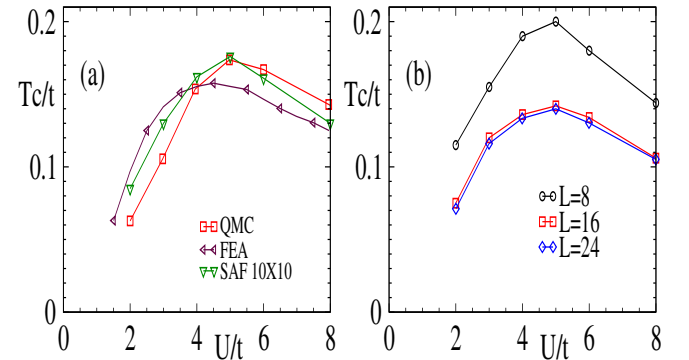


FIG. 7. Colour online: (a) Comparison of our  $T_c$  (labelled SAF) with QMC on a  $10 \times 10$  lattice, and the semi-analytic method employing the fluctuation exchange approximation (FEA)<sup>9</sup>. DMFT results<sup>25</sup> overestimate the  $T_c$  significantly, and also the location of peak  $T_c$ , and have not been included in the same plot. (b) Size dependence of our result, showing that the  $T_c$  estimate is almost size independent after  $L = 16$ .

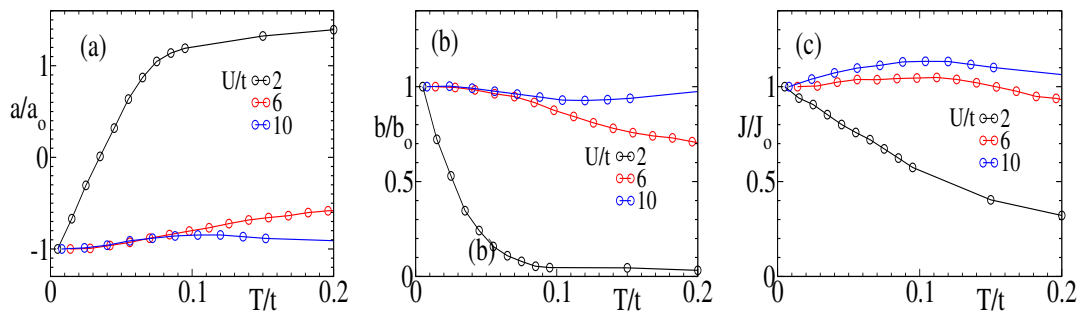


FIG. 8. Colour online: Parameters defining the phenomenological model. (a) The parameter  $a(T, U)$ , (b) the parameter  $b(T, u)$ , and (c) the stiffness  $J(T, U)$  of the effective XY model for the phase degrees of freedom.  $a$  and  $b$  are normalized to their  $T = 0$  values. Notice the essential flatness of  $a(T)$  and  $b(T)$  at  $U = 10t$ , the weak  $T$  dependence at  $U = 6t$ , and the dramatic variation with  $T$  at  $U = 2t$ .  $J$  similarly is only weakly  $T$  dependent for  $U \gtrsim 6t$  and varies strongly with  $T$  at weak coupling.

of  $t/\Delta$ , leading to the strong coupling limit:

$$H_{eff}^{\infty}\{\Delta_i\} \approx -t^2/|\Delta| \sum_{\langle ij \rangle} \cos(\theta_i - \theta_j) + \sum_i H_{loc}(|\Delta_i|)$$

$H_{loc}(|\Delta_i|)$  can be obtained from the atomic problem. The leading intersite term is calculated perturbatively and connects only nearest neighbour sites.

While these BCS and BEC limits are easy, obtaining an usable functional at arbitrary  $U/t$  does not seem possible. We have therefore tried a parametrisation of the (local) amplitude fluctuation spectrum and the phase correlations in terms of the following phenomenological model. It is valid at all  $U/t$  and over the temperature window of interest.

$$H_{eff}^{phen} = - \sum_{\langle ij \rangle} J \cos(\theta_i - \theta_j) + \sum_i \{a|\Delta_i|^2 + b|\Delta_i|^4\}$$

The first term defines an effective XY model involving only the phases, but, as we will see, the  $J$  needs to be temperature dependent to incorporate the effect of amplitude fluctuations. The amplitude part of  $H_{eff}$  is purely local, and to that extent misses out on spatial correlation between amplitude fluctuations.

The parameters  $a$  and  $b$  are extracted from a fit to the  $P(|\Delta|)$  that we obtain from the full MC, see Fig.3. With the moments of  $|\Delta_i|$  fixed by  $a$  and  $b$ , the  $J(U, T)$  is obtained by imposing the following equality:

$$\langle \sum_{ij} |\Delta_i| |\Delta_j| \cos(\theta_i - \theta_j) \rangle_{MC} = \langle \sum_{ij} |\Delta^2| \cos(\theta_i - \theta_j) \rangle_{phen}$$

The left hand side is the MC based order parameter, Fig.1(a). The right hand side computes the same quantity within the phenomenological model (in which the  $|\Delta|$  and  $\theta$  averages factorise) by using a Monte Carlo estimate of  $\langle \cos(\theta_i - \theta_j) \rangle$  in the XY model.

Fig.8.(a)-(b) shows the  $T$  dependence of  $a$  and  $b$  for  $U = 2, U = 6$  and  $U = 10$ . Because of the large difference in scales between the weak and strong coupling we have normalized the parameters by their  $T = 0$  values.

The  $U = 2t$  parameters show large change with  $T$ . The normalized  $a$  quickly increases and becomes positive, while  $b$  rapidly decreases from its  $T = 0$ . Both parameters tend to saturate for  $T \sim T_c \sim 0.07t$ . The 6th order term in the expansion would be necessary to describe the  $U = 2t$  case accurately.

With increasing  $U$ , the thermal change of the parameters slows down, and even at  $U = 6t$  the parameters show a much weaker dependence on  $T$ . By  $U = 10t$ , they are essentially constant at their  $T = 0$  values, indicating that only phase fluctuations are relevant in this regime.

To gain more perspective, we consider an expansion of the distribution about its mean value,  $P(\Delta) = K_2(\Delta - \Delta_0)^2 + K_3(\Delta - \Delta_0)^3 + K_4(\Delta - \Delta_0)^4 \dots$ , where the first term represents the gaussian stiffness of the distribution and the other terms represent non gaussian contributions. At strong coupling, the physics is driven completely by the phase fluctuation term, and the magnitude of the amplitudes is almost fixed. Thus, the stiffness coefficient is very large. As the coupling decreases, amplitude fluctuations increase, hence signalling a decrease in the stiffness. Apart from the increase in amplitude fluctuations, the mean value of  $\Delta$  also shows a remarkable increase with  $T$  at weak coupling, signalling the importance of the non gaussian terms in the expansion. We next turn to examine the phase stiffness which is the crucial coupling at large  $U$ .

Fig.8.(c) shows the  $T$  dependence of  $J$  for the three couplings, again normalized by their  $T = 0$  values,  $J_0(U)$ . The  $U = 2t$  case shows a pronounced decrease with  $T$ , while the other two are effectively constant. An XY description with a  $T$  independent coupling is reasonable for  $U = 6t$  and  $10t$  but inadequate at  $U = 2t$ .

*Role of the ‘density’ field:* An important addition in our model is the field  $\phi$ , coupling to the density operator. It serves a twofold purpose: first, it is indispensable in a disordered system since it provides a site dependent background field that renormalises the total disorder, and is crucial to get the correct scales; and second, it incorporates fluctuations in the charge sector, which play an important role for  $n \sim 1$ .

At  $n = 1$  the negative  $U$  Hubbard model can be mapped to its positive  $U$  counterpart, with the components of the magnetization field,  $\mathbf{m}_i$  of the positive  $U$  model corresponding to the  $\Delta_i$  and  $\phi_i$ . The symmetry the model is increased from  $O(2)$  to  $O(3)$ , and hence, there can be no superconducting order at finite temperature in 2D. At  $T = 0$ , the superconducting state is degenerate with the charge density wave state. This degeneracy is built into the structure of our model, and simulations at  $n \sim 1$  do actually show both superconductivity and charge density wave order at low  $T$ . The two field decomposition captures the correct ground state and relevant fluctuations in the model.

*Handling inhomogeneity:* As remarked earlier, this method is particularly well suited to dealing with inhomogeneous systems, including disordered systems and systems in a trap. We have extensively studied both of these, the former in the context of the disorder induced superconductor-insulator transition<sup>41,42</sup>, and the latter in the context of superconductors in a harmonic trap<sup>43</sup>. In such inhomogeneous systems, the Hartree feedback plays a crucial role in modifying the effective potential that the electronic system sees. In the former, this is crucial in determining the correct critical disorder and moderate disorder charge transport properties<sup>41</sup>, and plays a major role in the spatial fragmentation of the system<sup>42</sup>. In a harmonic trap, the resultant inhomogeneous density profile can drastically alter the spectral properties of the system<sup>43</sup>, compared to a flat one. Similarly for FFLO phases in imbalanced Fermi systems the real space treatment on large lattices allow access to a wealth of non trivial modulated phases.

*Quantum fluctuations:* The major approximation in our model is the neglect of temporal fluctuations in the auxiliary fields. The primary effect is the absence of low energy ‘bosonic’ modes (due to preformed pairs) at strong coupling. This does not affect the thermodynamics and

single particle spectrum significantly. Two particle correlations like conductivity also give accurate results as long as we are at moderate  $U$ . However, as we increase  $U/t$  the system develops a pseudo-gap (or a gap) above  $T_c$ , and we get a resistivity with steadily increasing insulating character. In the complete treatment the bosonic modes allow a parallel channel of conduction. A purely static approximation misses this contribution at large  $U/t$ , as does DMFT.

## VI. CONCLUSIONS

We have presented results on BCS-BEC crossover in an attractive Fermi system in the context of the two dimensional Hubbard model. We use an auxiliary field decomposition, treat these fields as classical, and solve the resulting problem through a real space Monte Carlo technique. The inclusion of all spatial thermal fluctuations allows us to capture the correct  $T_c$  all the way from the BCS to the BEC end. It allows conceptual clarity about the amplitude and phase fluctuation dominated asymptotes and the crucial intermediate coupling window where both these fluctuations are relevant. We provide a detailed characterisation of the auxiliary field behaviour that dictates fermion physics and access results on the density of states and angle resolved spectral features without any need for analytic continuation. We lay the groundwork for the study of disordered superconductors, trapping effects in superfluids, and spontaneous inhomogeneity in imbalanced systems.

*Acknowledgments:* We acknowledge use of the High Performance Computing Cluster at HRI. PM acknowledges support from a DAE-SRC Outstanding Research Investigator Award.

- 
- <sup>1</sup> For a recent review, see Q. Chen, J. Stajic, S. Tan and K. Levin, Phys. Repts. **412**, 1 (2005).
- <sup>2</sup> J. Bardeen, L. N. Cooper, and J. R. Schrieffer, Phys. Rev. **108**, 1175 (1957).
- <sup>3</sup> D. M. Eagles, Phys. Rev. **186**, 456 (1969).
- <sup>4</sup> A. J. Leggett in *Modern Trends in the Theory of Condensed Matter*, Springer-Verlag, Berlin.
- <sup>5</sup> P. Nozieres and S. Schmitt-Rink, J. Low. Temp. Phys. **59**, 195 (1985).
- <sup>6</sup> Daniel Rohe and Walter Metzner, Phys. Rev. B **63**, 224509 (2001).
- <sup>7</sup> For an early review, see R. Micnas, J. Ranninger and S. Robaszkiewicz, Rev. Mod. Phys. **62**, 113 (1990).
- <sup>8</sup> M. Randeria in *Bose-Einstein Condensation*, Cambridge University Press (1995).
- <sup>9</sup> J. J. Deisz, D. W. Hess, and J. W. Serene, Phys. Rev. **B66**, 014539 (2002).
- <sup>10</sup> H. Tamaki, Y. Ohashi and K. Miyake, Phys. Rev. **A77**, 063616 (2008).
- <sup>11</sup> B. Kyung, S. Allen, and A.-M. S. Tremblay, Phys. Rev. **B64**, 075116 (2001).
- <sup>12</sup> N. Dupuis, Phys. Rev. B **70**, 134502 (2004).
- <sup>13</sup> T. K. Kopec, Phys. Rev. B **65**, 054509 (2002).
- <sup>14</sup> R. T. Scalettar, E. Y. Loh, J. E. Gubernatis, A. Moreo, S. R. White, D. J. Scalapino, R. L. Sugar and E. Dagotto, Phys. Rev. Lett. **62**, 1407 (1989).
- <sup>15</sup> A. Moreo and D. J. Scalapino, Phys. Rev. Lett. **66**, 946 (1991).
- <sup>16</sup> A. Moreo, D. J. Scalapino and S. R. White, Phys. Rev. **B45**, 7544 (1992).
- <sup>17</sup> M. Randeria, N. Trivedi, A. Moreo, and R. T. Scalettar, Phys. Rev. Lett. **69**, 2001 (1992).
- <sup>18</sup> N. Trivedi and M. Randeria, Phys. Rev. Lett. **75**, 312 (1995).
- <sup>19</sup> S. Allen, H. Touchette, S. Moukouri, Y. M. Vilch and A. M. S. Tremblay. Phys. Rev. Lett. **83**, 4128 (1999).
- <sup>20</sup> J. M. Singer, T. Schneider and P. F. Meier, EPJB **7**, 37 (1999).

- <sup>21</sup> A. Sewer, X. Zotos and H. Beck, Phys. Rev. B **66**, 140504 (2002).
- <sup>22</sup> T. Paiva, R. R. dos Santos, R. T. Scalettar and P. J. H. Denteneer, Phys. Rev. B. **69**, 184501 (2004).
- <sup>23</sup> T. Paiva, R. Scalettar, M. Randeria and N. Trivedi, Phys. Rev. Lett. **104**, 066406 (2010).
- <sup>24</sup> K. Bouadim, *et al.*, Nat. Phys. **7**, 884 (2011).
- <sup>25</sup> M. Keller, W. Metzner and U. Schollwöck, Phys. Rev. Lett. **86**, 4612 (2001).
- <sup>26</sup> M. Capone, C. Castellani and M. Grilli, Phys. Rev. Lett. **88**, 126403 (2002).
- <sup>27</sup> A. Garg, H. R. Krishnamurthy and M. Randeria, Phys. Rev. B **72**, 024517 (2005).
- <sup>28</sup> J. Bauer and A. C. Hewson, Europhys. Lett. **85** 27001 (2009).
- <sup>29</sup> J. Bauer, A. C. Hewson and N. Dupuis, Phys. Rev. B **79**, 214518 (2009).
- <sup>30</sup> A. Koga and P. Werner, Phys. Rev. A **84**, 023638 (2011).
- <sup>31</sup> V. F. Gantmakher and V. T. Dolgoplov, Phys. Usp. **53**, **3** (2010).
- <sup>32</sup> I. Bloch, Nat. Phys. **1**, **23** (2005), I. Bloch, *et al.*, Rev. Mod. Phys. **80**, **885** (2008).
- <sup>33</sup> S. Giorgini, *et al.*, Rev. Mod. Phys. **80**, **80**, 1215 (2008), R. Casalbouni, *et al.*, Rev. Mod. Phys. **76**, 263 (2004), X-Wen Guan, *et al.*, Rev. Mod. Phys. **85**, 1633 (2013)
- <sup>34</sup> F. Solms, H. G. Miller and R. M. Quick, Phys. Rev. B **49**, 15945 (1994).
- <sup>35</sup> Look at supplementary material, in K. Bouadim, Y. L. Loh, M. Randeria and N. Trivedi, arxiv: 1011.3275
- <sup>36</sup> G. J. Conduit and Y. Meir, Phys. Rev. B **84**, 064513 (2011).
- <sup>37</sup> Y. Dubi, *et al.*, Nature, **449**, 876 (2007).
- <sup>38</sup> M. Mayr, G. Alvarez, C. en, and E. Dagotto, Phys. Rev. Lett. **94**, 217001 (2005).
- <sup>39</sup> P. G. de Gennes, *Superconductivity of metals and alloys*, Addison Wesley (1989).
- <sup>40</sup> S. Kumar and P. Majumdar, Eur. Phys. J. B, **50**, 571 (2006).
- <sup>41</sup> S. Tarat and P. Majumdar, arXiv:1311.6951
- <sup>42</sup> S. Tarat and P. Majumdar, to be published
- <sup>43</sup> Sanjoy Datta, Viveka Nand Singh and Pinaki Majumdar, arXiv:1312.5761